J Oceanogr (2012) 68:485–496
DOI 10.1007/s10872-012-0113-0

REVIEW

Variability of the Bering Sea circulation in the period 1992–2010

Gleb Panteleev · Max Yaremchuk · Vladimir Luchin · Dmitri Nechaev · Takashi Kukuchi

Received: 11 September 2011 / Revised: 6 April 2012 / Accepted: 14 April 2012 / Published online: 9 June 2012

Abstract Sea surface height anomalies observed by satellites in 1992–2010 are combined with monthly climatologies of temperature and salinity to estimate circulation in the southern Bering Sea. The estimated surface and deep currents are consistent with independent velocity observations by surface drifters and Argo floats parked at 1,000 m. Analysis reveals 1–3-Sv interannual transport variations of the major currents with typical intra-annual variability of 3–7 Sv. On the seasonal scale, the Alaskan Stream transport is well correlated with the Kamchatka (0.81), Near Strait (0.53) and the Bering Slope (0.37) currents. Lagged correlations reveal a gradual increase of the time the lags between the transports of the Alaskan Stream, the Bering Slope Current and the Kamchatka Current, supporting the concept that the Bering Sea basin is ventilated by the waters carried by the Alaskan Stream south of the Aleutian Arc and by the flow through the Near Strait. Correlations of the Bering Sea currents with the Bering Strait transport are dominated by the seasonal cycle. On the interannual time scale, significant negative correlations are diagnosed between the Near Strait transport and the Bering Slope and Alaskan Stream currents. Substantial correlations are also diagnosed between the eddy kinetic energy and Pacific Decadal Oscillation.

Keywords Bering Sea · Inter-annual variability · Sea surface height · Volume transport · Aleutian passes · Kinetic energy

G. Panteleev (✉)
International Arctic Research Center (IARC),
University of Alaska, Akasofu Building,
Fairbanks, AK 99975, USA
e-mail: gleb@iarc.uaf.edu

M. Yaremchuk
Naval Research Laboratory, Stennis Space Center,
Hancock, USA

V. Luchin
V.I.Il'ichev Pacific Oceanological Institute, Far Eastern Branch,
Russian Academy of Sciences (POI FEB RAS),
43 Baltiyskaya Street, 690041 Vladivostok, Russia

D. Nechaev
Department of Marine Science, University of Southern
Mississippi, Hattiesburg, USA

T. Kukuchi
Japan Agency for Marine-Earth Science and Technology,
Yokosuka, Japan

1 Introduction

Transport of waters in the Bering Sea (BS) plays an important role in the exchange of properties between the Pacific and Arctic oceans. Therefore, monitoring long-term variations of the BS currents and their relations between each other and the atmosphere may provide a better understanding of the mechanisms controlling regional and global climate change phenomena (Luchin et al. 2002; Overland and Stabeno 2004).

Recent modeling (Clement et al. 2005; Maslowski et al. 2008; Clement Kinney et al. 2009; Hu and Wang 2010) and observational (Mizobata et al. 2002, 2006) studies suggest, in particular, that mesoscale eddies play a decisive role in the exchange of properties between the northern BS shelf and the southern BS basin, thus controlling transport of the Pacific waters into the Arctic Ocean. Process studies by Wang and Ikeda (1997) and Zhang et al. (2011) confirm the importance of mesoscale instabilities along sloping topography and their ability to strongly affect local large-scale circulation along the BS shelf break. Equally

important are transports of the larger-scale components of the BS circulation, primarily driven by winds and the Alaskan Stream inflow into the basin at the southern open boundary. Due to significant uncertainties of the forcing fields, numerical estimates of the large-scale transports in the BS system are subject to large uncertainty in the literature. As an example, the mean transport of the Kamchatka Current varies from 10–14 Sv (Stabeno et al. 1999) to 20–25 Sv (Panteleev et al. 2006; Hu and Wang 2010) in the numerical studies with 9–18-km resolution. New massive sources of data (satellite altimetry, Argo drifters) may improve the accuracy of these estimates in the near future.

Large-scale circulation features in the deep basins of the BS were estimated from observations by many authors (e.g., Reed 1984; Verkhunov and Tkachenko 1992; Reed et al. 1993; Stabeno et al. 1999) who primarily used dynamic topography maps relative to 500–1,500 dbar derived from available hydrological stations. Development of satellite technologies introduced massive sources of information coming from drifters and altimeters, which enabled direct observations of both the surface (Stabeno and Reed 1994) and deep (Johnson et al. 2004) circulation features. In particular, observations of deep currents by Argo drifters have shown that circulation at 1,000 m provides a substantial, if not primary, contribution to the total transport and, therefore, should not be neglected in the computations.

Satellite altimeters supply information on the BS surface geostrophic currents for more than 2 decades. Combining these data with in situ observations of temperature, salinity and subsurface currents allowed obtaining increasingly accurate estimates of the Bering Sea mean dynamic topography (MDT) (Panteleev et al. 2011), which indicated that the major current systems in the Bering Sea and surroundings are stronger than those deduced from hydrological surveys using the assumption of no motion at 1,000–1,500 m. In particular, Panteleev et al. (2006) estimated the Kamchatka Current transport of 24 Sv (1 Sv $= 10^6$ m^3/s), a value significantly higher than previous estimates of Stabeno and Reed (1992) and Verkhunov and Tkachenko (1992) referenced to 1,500 dbar. Similar indications of stronger transports were obtained by Cokelet et al. (1996), who analyzed ADCP-referenced geostrophic circulation in the deep basin of the BS, and by Hughes et al. (1974), who estimated transports of the Near and Bering Straits from surface drifters and CTD sections.

Recent results of the long-term moored velocity measurements in the major straits of the Aleutian Arc also indicate a significant contribution of the deep currents: using the results of 4-year moored observations in the Amukta Pass Stabeno et al. (2005) estimated its transport as 4 ± 1 Sv, which is almost seven times higher compared to the previous indirect estimates, obtained from hydrological station data (Stabeno et al. 1999). More recent observations in the Amukta Pass have shown even higher northward tranport of 4.7 Sv into the Bering Sea (Ladd and Stabeno 2009).

In this study we try to obtain a 18-year-long estimate of the BS circulation from the Aviso altimetry (http://www.aviso.oceanobs.com), historical station data and drifter observations. To reduce the unrealistically strong near-bottom currents that routinely emerge when the dynamical method is referenced to the sea surface, we utilize monthly temperature/salinity climatologies adjusted to the original stations, drifter and atmospheric data by means of the dynamically constrained variational interpolation technique (Panteleev et al. 2006, 2011). The impact of mesoscale eddies, unresolved by the climatologies, is accounted for by the Cooper-Haines (1996) algorithm.

The article is organized as follows: In the next section we describe the data sets used, their pre-processing and error analysis techniques. In Sect. 3 the results of the flow field reconstruction in the ice-free regions of the BS are presented and validated against independent drifter data. In the same section we analyze correlations between the transports of the major BS currents, including an independent estimate of the Bering Strait transport derived from 10-year moored observations by Woodgate et al. (2005). Reconstructed flow field anomalies are also used to analyze intra-seasonal variations of the eddy kinetic energy and to establish correlations with atmospheric forcing on interannual scales parameterized by the Pacific Decadal Oscillation (PDO). Section 4 summarizes the results of the study.

2 Data and methods

2.1 Aviso altimetry

Since 1992, the ocean surface topography has been continuously observed from space by the Topex/Poseidon, European Remote Sensing (ERS), Geosat Follow-On (GFO), Envisat and Jason satellite missions. These data are available at http://www.aviso.oceanobs.com. In this study the gridded sea surface height anomalies (SSHA) for the period of 1992–2010 were used to define a reference pressure for the diagnostic computations.

For each 7-day period, the SSHAs, obtained by optimal interpolation of all the available altimeter missions, were downloaded from the Aviso site together with the respective error estimates. The latest version of the product is derived using anisotropic and spatially inhomogeneous covariance functions with an improved statistical error model, accounting for subgrid motions and various types of long wavelength errors (Pascual et al. 2006). Every week

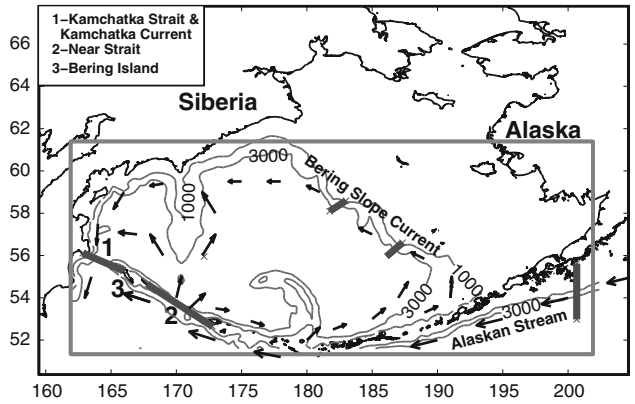

Fig. 1 Schematics of the BS circulation. *Bold rectangle* shows the domain of the diagnostic computations. *Thick gray lines* show the sections across the key circulation features, where weekly transports were estimated. Topography contours of 1,000 and 3,000 m are shown

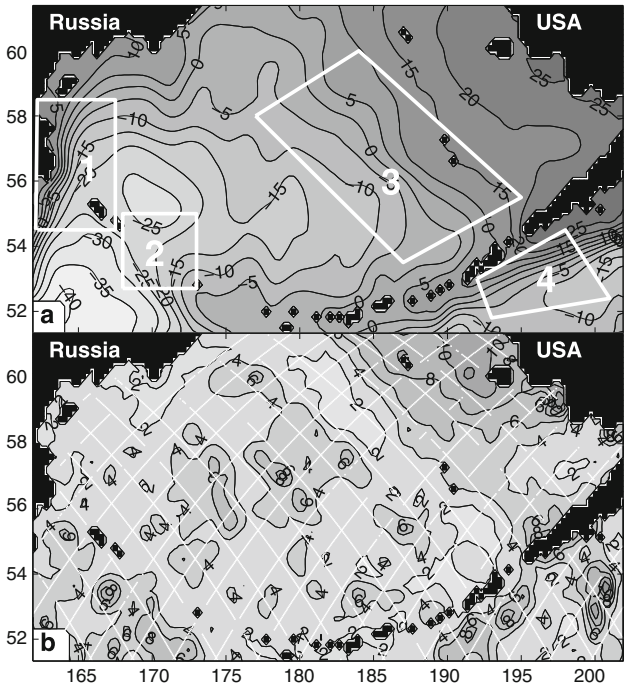

Fig. 2 The climatological mean SSH field (**a**) and the snapshot of the total SSH error field on 1 April 2000 (**b**). *White quadrangles in the upper panel* show averaging areas of the drifter data in the KC (*1*), NS (*2*), BSC (*3*) and AS (*4*) regions used in the validation experiments (Table 1)

the gridded Aviso SSHA and the respective error fields were interpolated from the original 1/3° × 1/3° grid on the model grid with 18 km (approximately 1/3° × 1/6°) horizontal resolution (Fig. 1).

The horizontal resolution of the gridded SSHA is defined by the footprints of the Topex-Poseidon and Jason-1 satellites (Fig. 2b). Although the along-track SSHA data have a resoluiton of approximately 8 km, the distance between the tracks is about 100 km, thus limiting the effective resolution of the Aviso product by 20–30 km. Because of this, the gridded Aviso SSHA can be used for analysis of the circulation in the Kamchatka and Narrow straits, but does not resolve narrow Aleutian Passes (Fig. 2b), which, in addition, are characterized by higher errors associated with the detiding procedure of the raw along-track observations. For this reason the overall accuracy of the Aviso product data is generally higher for the deep regions where the tidal signal is smaller. Aviso data have been successfully used for analysis of the BS circulation (e.g., Foreman et al. 2004; Chernyawsky et al. 2004, 2005; Mizobata et al. 2010).

Being highly accurate (∼2–3 cm) in retrieving the time-dependent component of SSH variability, the mean SSH provided by satellites still suffers from significantly larger errors (∼10–20 cm) of geoid models (e.g., Elmann 2010). To derive the absolute SSH maps, the gridded Aviso anomalies were added to the Bering Sea mean dynamic topography (MDT, Fig. 2a) obtained by combining all available observations with dynamical constraints in the framework of the variational data assimilation approach (Panteleev et al. 2011). The respective MDT and SSHA error fields were assumed to be uncorrelated, and the resulting errors varied between 1 and 10 cm (Fig. 2b) with the mean magnitude of 2.9 cm in the deep part of the BS basin.

2.2 Argo and surface drifters

Drifter data were used in the study for validation purposes and consisted of two major components: surface and subsurface (Argo) drifters.

Surface drifters included 497 trajectories from the Fisheries Oceanography Coordinated Investigations (FOCI) data base http://www.pmel.noaa.gov/foci and 84 drifter trajectories from the Global Drifter Program (GDP) data base http://www.aoml.noaa.gov/phod/dac/ observed during 1992–2004. The FOCI surface drifters were drogued at 40 m, and GDP drifters had drogues at 15 m. Most (86 %) of the these velocity data were obtained from FOCI drifters driven by currents below the Ekman layer due to a relatively deep drogue. Preliminary analysis of these observations included low-pass filtering of the trajectories with a 1-week cutoff period and velocity estimation by taking the difference between the drifter's positions. The root-mean-square (rms) error variance ranged from 0.05 to 0.2 m/s depending on the drifter location.

Velocity data from Argo drifters (Wilson 2000) were taken from http://apdrc.soest.hawaii.edu/projects/yomaha/yomaha07. This data set included 1994 velocity estimates at 1,000 m spanning the period from May 2001 to April 2007. The mean duration of an Argo drifter residence at the parking depth was 8.9 days, with 90 % of the values

ranging in between 8.2 and 10.3 days. The mean displacement of a drifter at 1,000 m was 35 km, giving a rough mean speed estimate of 4.3 cm/s. The mean velocity at the parking depth was estimated by taking the difference between drifter coordinates before the dive and immediately after resurfacing. The respective error σ_d combines an estimate of the drifter's displacement during the ascent/descent phase with an estimate of surface velocity acquired from the drifter's position fixes at the surface (more details can be found on the YoMaHa website). The mean value of σ_d in the region was found to be 3.1 cm/s.

2.3 Temperature and salinity

Computation of geostrophic currents by integrating density from the surface results in severe violation of the kinematic constraints imposed on the velocity field by the bottom. A standard way to improve the accuracy is to start integration from a reference level (1–1.5 km), assuming that pressure anomalies are negligible there. Such a procedure provides the SSH value under an implicit assumption of the error-free density in the water column (Fomin 1964).

In the present study the mesoscale density anomalies ρ' are largely unknown, whereas the mean density field ρ could be determined with a reasonable accuracy from historical observations. The hydrological database at our disposal contains 56,342 temperature and salinity profiles collected in the Bering Sea between 1932 and 2004 (see Panteleev et al. 2011 for more details). These observations were assimilated together with drifter and atmospheric forcing data into a regional primitive-equation model (Panteleev et al. 2006, 2011) to obtain dynamically consistent estimates of the climatological distribution of the of ρ and ζ in the region. A similar technique was used to obtain seasonal climatologies for density.

A posteriori errors $\sigma_\rho, \sigma_\zeta$ of the mean fields were computed by estimating the diagonal elements of the Hessian matrix associated with the assimilation problem. Their values varied within 10–30 % of the respective mean values. The dynamically optimized density climatologies were then linearly interpolated in time to obtain weekly fields of ρ, which were corrected for unresolved mesoscale signal ρ' and combined with ζ and ζ' to diagnose velocity.

2.4 Velocity estimation

To obtain a realistic velocity field with the diagnostic method, one has to account for the density variations ρ' associated with the mesoscale eddies, which are absent in the seasonal climatologies, but are implicitly present in Aviso SSH anomalies ζ'. In this study, ζ' was projected on ρ' by the means of the Cooper-Haines (1996) technique,

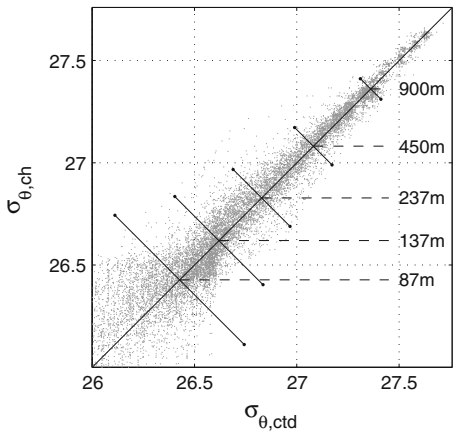

Fig. 3 *Scatter plot* of the diagnosed density field against in situ observations in the Bering Sea during 2002. *Slanted bars* show observed rms variations of the BS density field at selected depths

widely used in sequential data assimilation schemes: the density profiles $\rho(z) + \rho'(z)$ were obtained by vertical displacement of $\rho(z)$ to cancel bottom pressure anomalies induced by ζ'. The pressure field p was computed by

$$p = g\rho_0(\zeta + \zeta') + g\int_{-h}^{0}(\rho + \rho')\mathrm{d}z, \quad (1)$$

where h is the local depth, g is the gravitational acceleration, ρ_0 is the water density at the surface, and $\rho'(z)$ is the Cooper-Haines correction to the background climatological density profile $\rho(z)$.

To validate the approach, we compared the diagnosed density $\rho + \rho'$ with in situ observations taken during 4 years (1997, 1998, 2002, 2003) of the most abundant observations in the 1990s and 2000s. As an example, Fig. 3 compares the diagnosed density with the density data from 678 CTD stations occupied in 2002. The depth-averaged correlation coefficient for this year is 0.71, whereas the difference between the observed and diagnosed densities (rms deviation of the points from the diagonal) is several times smaller than the typical rms variation of the density field at a given level shown by slanted bars. Other years demonstrated similar distributions with the correlation coefficients of 0.61 (1997), 0.63 (1998) and 0.67 (2003). These estimates show that the adopted diagnostic method provides mesoscale density variations with an accuracy of 30–40 %, which is sufficient for statistical analysis of the velocity field in the major part of the investigated region, including the all sections shown in Fig. 1.

At any given moment this approach keeps the water mass structure intact, conserves potential vorticity and avoids violation of the kinematic boundary condition at the bottom, because mesoscale velocity at $z = -h$ is zero,

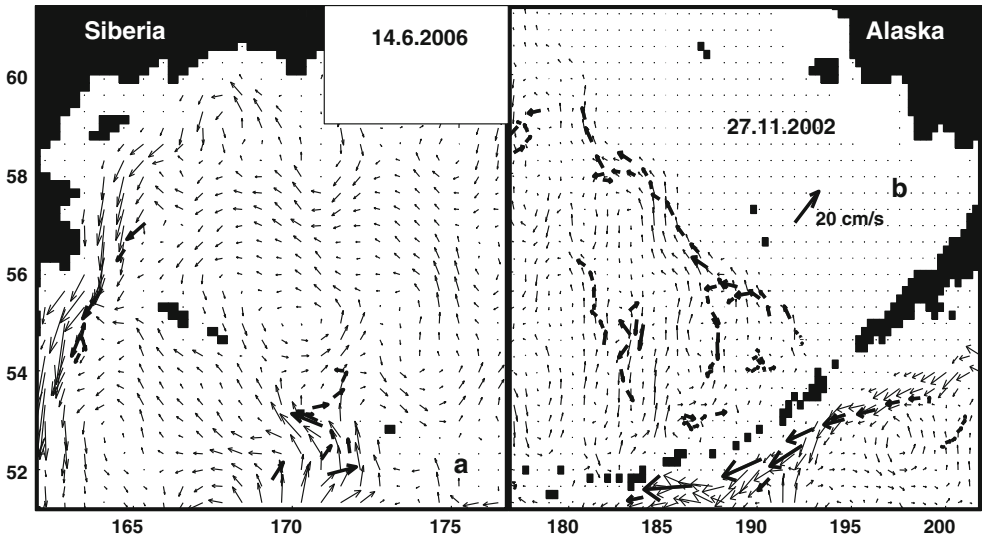

Fig. 4 The snapshots of the horizontal velocities (*thin arrows*) at 1,000 m in the eastern and western parts of the BS. *Thick arrows* show velocity of the Argo floats within the temporal window of 70 days with respect of the day designated in the subplots

whereas the climatological fields ζ and ρ are dynamically balanced by the variational assimilation algorithm.

Weekly velocity vectors v were computed by applying the geostrophic relationships to the pressure field given by Eq. (1):

$$\boldsymbol{v} = -\frac{1}{f\rho_0}\mathbf{k} \times \nabla p, \tag{2}$$

where f is the Coriolis parameter, and $\mathbf{k}$ is the vertical unit vector.

Figure 4 compares the velocities estimated from Eq. (1, 2) with those and velocities derived from Argo floats parked at 1,000 m. Qualitatively, the best agreement is observed in the Kamchatka Strait and in the Alaskan Stream where strong currents are controlled by local topography. The agreement is worse in the Near Strait and in the eastern part of the BS where currents are weaker and eddy activity is stronger. Despite that, Fig. 4b suggests that reconstructed velocities resolve a significant part of the eddy activity observed by the Argo floats.

Equations (1, 2) do not guarantee the integral volume conservation. Despite this, we found that the northward flow through the northern boundary of the region ranged between 1.5 and −0.5 Sv, i.e., was fairly consistent with the observed variability of the Bering Strait transport (Woodgate et al. 2005). Such a reasonable behavior could be partly attributed to the dynamical balance between the MDT and the climatological density fields.

Velocity errors were estimated using the relationship

$$\mathsf{E}_{\mathbf{v}} = \mathsf{G}_{\mathbf{v}}^{T}\mathsf{E}\mathsf{G}_{\mathbf{v}}, \tag{3}$$

where $\mathsf{G}_{\mathbf{v}}$ is the matrix of discrete representation of the diagnostic operator (Eqs. 1, 2), mapping SSH and density on the velocity, and E is the diagonal matrix of the SSH and density error variances $\sigma_\rho^2, \sigma_\zeta^2$.

3 Results

3.1 Validation against drifter and mooring data

To check the consistency of the diagnosed velocity fields, we compared their weekly values with the drifter data described in Sect. 2.2.

Prior to comparison with the Argo data, velocity fields at 1,000 m were smoothed with the 25-km-wide Gaussian filter centered at the average drifter location between its position fixes at the surface. Figure 5b shows the scatter plot of the computed velocity $\boldsymbol{v}$ against the respective and Argo floats $\boldsymbol{u}$ velocity. Given the relatively large errors in determination of both the drifter (3.1 cm/s) and diagnosed (5.3 cm/s) velocities, their magnitudes coincide at the 85 % confidence level.

We also computed the canonical correlation coefficient c (Schrier 2008) between $\boldsymbol{u}$ and $\boldsymbol{v}$

$$c = 1 - \det\left[\mathsf{I} - \mathsf{C}_{vv}^{-1}\mathsf{C}_{uv}\mathsf{C}_{uu}^{-1}\mathsf{C}_{uv}^{T}\right]. \tag{4}$$

Here C stands for the covariance matrix between the subscript vectors, T denotes transposition and I is the 2×2 identity matrix. The coefficient c is normalized in a way that $0 \le c \le 1$ and measures the degree of linear dependence between $\boldsymbol{u}$ and $\boldsymbol{v}$. The resulting value $c = 0.42$ is different from zero at the 90 % confidence level and appears satisfactory, given the uncertainties in the determination of $\boldsymbol{u}$ and $\boldsymbol{v}$.

Correspondence between the surface drifter velocities $\boldsymbol{u}_s$ and $\boldsymbol{v}$ appears somewhat better (Fig. 5a), possibly because of the absence of errors introduced by the Cooper-Haines corrections to the density field during calculation of the dynamic height and its derivatives. The magnitudes of $\boldsymbol{u}_s$ and $\boldsymbol{v}$ differ insignificantly with the 95 % confidence. The respective correlation coefficient (4) is also higher (0.48) than for the Argo drifters (Fig. 5).

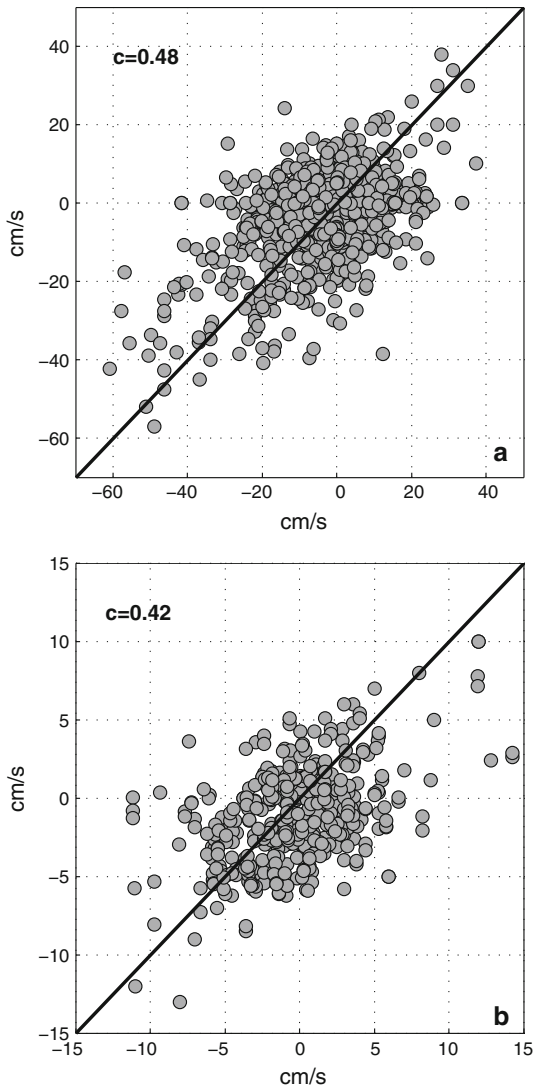

Fig. 5 Scatter plots of the surface (**a**) and Argo (**b**) drifter velocity components (*vertical axes*) against the reconstructed velocity components (*horizontal axes*) at 30 and 1,000 m. Correlation coefficients are shown. Velocity values are in cm/s

Table 1 compares the mean velocity magnitudes in the four key regions of the Bering Sea shown in Fig. 2a. The relative difference between the mean velocity magnitudes is 5 % for the Argo drifters and 17 % for the surface drifters. A larger discrepancy with surface drifters can be partly explained by the contribution of the Ekman flow (especially to the GDP drifters), which may also be responsible for larger magnitudes of the surface drifter velocities compared to the diagnosed geostrophic velocity (two lower lines in Table 1). Indications of the large Ekman transport, especially in winter, have been well documented by both experimental (Stabeno et al. 1999) and numerical (Hu and Wang 2010) studies of the BS.

Overall, the results of validation show that the reconstructed weekly velocity fields are consistent with independent drifter observations and can be used for further statistical analysis of the key integral features of the circulation.

Table 1 Mean magnitudes (cm/s) of the reconstructed velocity vectors and the velocity vectors retrieved from drifter trajectories (shown in italic)

	Total	KC	NS	BSC	AS
Argo drifters	4.5	10.1	4.9	3.4	5.8
	4.4	*7.3*	*5.4*	*3.8*	*6.4*
Surface drifters	9.8	12.1	9.2	8.2	14.0
	11.8	*11.1*	*11.6*	*9.1*	*18.6*

Averaging is done separately for the entire domain (first column) and for the four key regions shown in Fig. 1

3.2 Transport anomalies

Geostrophic circulation in the Bering Sea is characterized as a cyclonic gyre driven by the inflow of the Alaskan Stream water through the numerous straits of the Aleutian Arc. The major portion of the inflow recirculates in the deep southwestern basin within the Bering Slope Current and exits through the Kamchatka Strait (Stabeno et al. 1999). Several percent of the gyre transport enter the northeastern BS shelf to form the Bering Strait outflow into the Arctic Ocean.

Although qualitatively this circulation pattern has been known for decades, transports of its major branches and their variability (except for the Bering Strait) remain highly uncertain because of the lack of direct observations of the deep currents. The diagnosed circulation sheds new light on the dynamics of the BS gyre and its variability on decadal to monthly time scales.

Figure 6 demonstrates the time series of the transports through the sections shown in Fig. 1: the Kamchatka current (KC), the Near Strait transport (NS), the Bering Slope Current (BSC) and the Alaskan Stream (AS). For better comparison with the result of Johnson et al. (2004), the BSC transports are averaged over two southwestward sections, starting from the 1,000 m isobath (Fig. 1).

A remarkable feature of the curves in Fig. 6 is relatively high amplitude of the transport variations compared to their mean values. The KC transport reached its maximum of 38.5 Sv in January 1998, while its 20-year minimum was only 6 Sv in May 1993, a value, statistically indistinguishable from zero. Similar extremes of the KC transport were obained by Hughes et al. (1974) and Verkhonov and Tkachenko (1992).

The AS transport appears to be more steady with a typical seasonal variation of 7 Sv around the mean value of 24.3 Sv. The BSC transport exhibits much larger fluctuations, which even reversed their direction to a −1.2-Sv

southeastward flow in the beginning of March 1996. The mean value of the BSC transport, calculated above the 2,000 m is 7.3 Sv, is in a reasonable agreement with the value obtained by Johnson et al. (2004) whose diagnostic estimate of 5.8 ± 1.7 Sv was referenced to the velocity field derived from Argo drifters. Hu and Wang (2010) obtained a somewhat lower estimate of 5 Sv by integrating their model result between 1,000 and 200 m contours. The NS inflow into the Bering Sea has a typical seasonal variation of 4 Sv with a mean value of 11 Sv.

Table 2 contains correlation coefficients between the low- and high-pass filtered transports of the series shown in Fig. 6, and the similarly filtered Bering strait transport from observations of Woodgate et al. (2005). In all the cases the cosine window with the annual cutoff scale was used. The filtered series were subject to autocorrelation analysis, which diagnosed the decorrelation scales of approximately 8.7 weeks and 2 years for the high- and low-pass series, respectively. Using these estimates, we evaluated the number of independent points (degrees of freedom) in the 18-year filtered series as 108 and 9. These numbers were used to compute the confidence limits via Fischer transformation of the sample correlations.

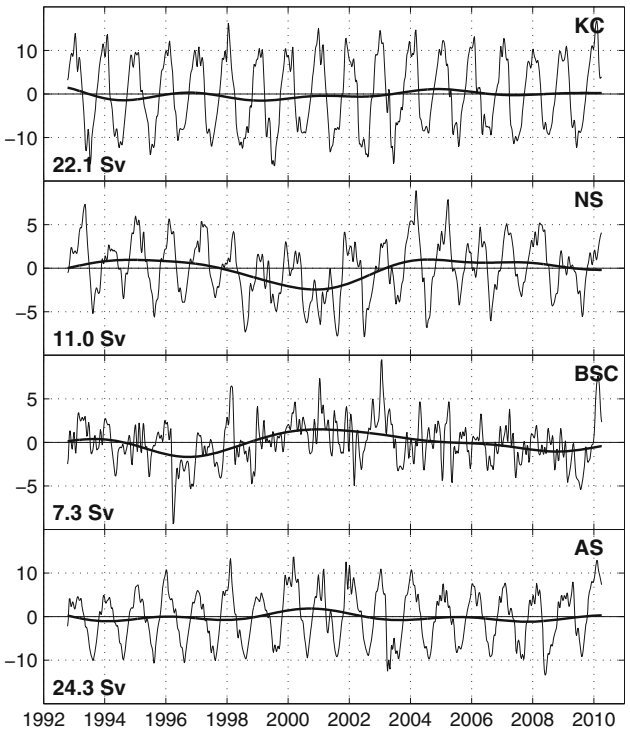

Fig. 6 Transport anomalies (Sv) of the Kamchatka Current (KC), the Near Strait (NS) throughflow, the Bering Slope Current (BSC) and the Alaskan Stream (AS). Low-pass filtered series are shown by *thick lines*. The mean values of transports are shown in the *left corners*

According to Table 2, the intra-annual correlations (above diagonal) with the Bering Strait transport are mostly negative. The result reflects domination of the seasonal signal in the series: it is well known that the Bering Strait transport reaches its maximum in summer and fall (e.g., Roach et al. 1995), whereas the BS circulation tends to spin up in winter (Fig. 5; Hughes et al. 1974). As a consequence of such intensification of the BS gyre, the mean SSH in the Bering Sea drops, reducing the large-scale sea level difference between the Pacific and Arctic Oceans that drives the Bering Strait transport on the interannual time scales.

Correlation estimates on the interannual time scales have an order of magnitude fewer degrees of freedom (e.g., 9 against 108 for the BS transports) and are much less confident: only three coefficients below the diagonal in Table 2 maintain their sign within the 95 % confidence limits. Among them are the correlations of the NS transport with the transports of the BSC (−0.67) and the AS (−0.84) (Table 2).

The third confident correlation is between the BSC and AS. Its value (0.58) appears to be larger than the intra-annual one (0.37), indicating that the teleconnection between these two currents across the Aleutian Arc is masked by eddy activity on the intra-annual scales.

Computation of the lagged correlations r among the transports of the AS, BSC and KC have shown that the time lags τ of maximum correlations gradually increase between the pairs AS-BSC ($r = 0.66$, $\tau = 0.9$ years), BSC-KC ($r = 0.8$, $\tau = 3.1$ years) and AS-KC ($r = 0.74$, $\tau = 4.4$ years). These numbers roughly correspond to the travel

Table 2 Correlations between the transports across the sections shown in Fig. 2

	KC			NS			BSC			AS			BStr		
KC		**1.00**		0.38	**0.53**	0.65	0.16	**0.34**	0.50	0.73	**0.81**	0.87	−0.203	**−0.44**	−0.63
NS	−0.33	**0.43**	0.85		**1.00**		0.12	**0.30**	0.46	0.62	**0.72**	0.80	−0.09	**−0.35**	−0.56
BSC	−0.50	**−0.25**	0.78	−0.11	**−0.67**	−0.92		**1.00**		0.20	**0.37**	0.52	−0.20	**−0.07**	−0.33
AS	−0.56	**0.16**	0.82	−0.40	**−0.84**	−0.97	0.13	**0.58**	0.90		**1.00**		−0.17	**−0.42**	−0.62
BStr	−0.87	**0.02**	0.88	−0.86	**−0.11**	−0.90	−0.87	**0.06**	0.89	−0.85	**−0.13**	0.91		**1.00**	

Matrix elements above the diagonal show correlations between the high-pass filtered transports retaining the seasonal cycle and shorter time scales. Low-pass filtered correlations on interannual time scales are shown below the diagonal. Boldfaced numbers show correlations. Numbers to the left and to the right show their 95 % confidence limits

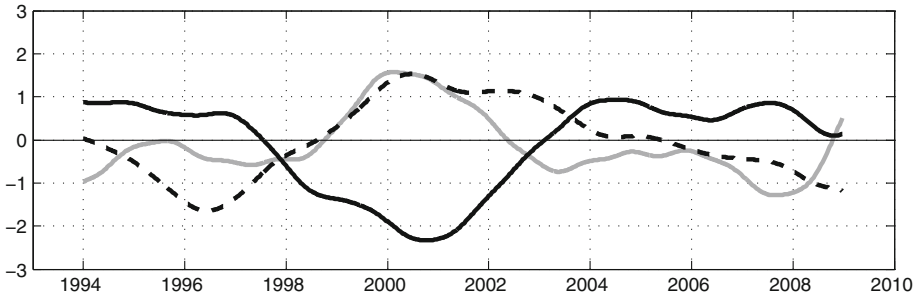

Fig. 7 Low-pass filtered transport anomalies (Sv) of the Bering Slope Current (*dashed line*), the Alaska Stream (*gray*) and the Near Strait throughflow

times along the pathways of the AS water in the BS basin with the mean depth-averaged velocity of approximately 2–3 cm/s. We assume that this result supports the concept that a significant portion of the AS is responsible for the deep ventilation of the Bering Sea basin.

Interestingly, the NS and KC transports correlate positively at zero lag ($r = 0.43$, Table 2) and negatively ($r = -0.72$) with the lag of 4.4 years. This is due to the high negative correlation ($r = -0.84$) between NS and AS transport at zero lag (Table 2) and a moderate positive ($r = 0.5$) correlation at the lags 4–5 years. The low-pass filtered BSC and NS transports in Fig. 7 have an opposite phase to the AS transport with a period of approximately 4–5 years. The origin of such behavior of the NS and AS transports is not quite clear, but one of the possibilities can be the formation of the large-scale eddies in the Alaskan Stream that block the transport of the AS water through the Aleutian Passes. A perfect example of this mechanism was described by Okkonen (1996).

Lagged correlation analysis suggests simple statistical relationships between the KC and BSC transports and NS and AS transports:

$$T_{\mathrm{KC}}(t) = 0.5T_{\mathrm{NS}}(t) + 0.26T_{\mathrm{AS}}(t-4.4) + \epsilon_{\mathrm{KC}} \quad (5)$$

$$T_{\mathrm{BSC}}(t) = -0.47T_{\mathrm{NS}}(t-1.1) + 0.3T_{\mathrm{AS}}(t-0.9) + \epsilon_{\mathrm{BSC}} \quad (6)$$

Here, for $T_{\mathrm{KS}}(t)$, $T_{\mathrm{BSC}}(t)$, $T_{\mathrm{NS}}(t)$, $T_{\mathrm{AS}}(t)$, are KS, BSC, NS and AS transports, t is the time in the years, and $\epsilon_{\mathrm{KS}}, \epsilon_{\mathrm{BSC}}$ are the stochastic errors. The relationships (5, 6) describe 89 and 77 % of the variability of the KS and BSC transports, respectively.

3.3 Eddy kinetic energy

Mesoscale variability is an important factor in the Bering Sea dynamics. Analysis of the moored velocity measurements along the eastern Alaskan continental slope (Schumacher and Reed 1992; Cokelet and Stabeno 1997) have shown mesoscale currents exceeding 80 cm/s, i.e., 10–15 times higher than the long-term mean BSC velocity. Eddy-induced across-shelf mixing is not well studied, although high mesoscale activity in the region indicates the importance of this mechanism. In particular, Mizobata et al. (2002, 2006) obtained evidence of the enhanced eddy-driven up-slope cross-shelf transport below 50 m in the BSC region with the opposite transport above. Earlier numerical experiments by Wang and Ikeda (1997) revealed a tendency for enhanced production of smaller scale eddies under the environment with a gently sloping southward bottom characteristic for the BSC region, whereas climatological simulations of Hogg et al. (2005) indicate a clear connection between the long-term variability of the large-scale dynamics and oceanic eddy activity.

Using the diagnosed velocity $\boldsymbol{v}$ fields at each level z_i, the depth-averaged eddy kinetic energy (EKE) was estimated by

$$\mathrm{EKE} = \frac{\rho_0}{2(z_2 - z_1)} \int_{z_1}^{z_2} (\boldsymbol{v} - \boldsymbol{v}_{\mathrm{cl}})^2 \mathrm{d}z, \quad (7)$$

Here $\boldsymbol{v}$ is the horizontal velocity vector derived as described above, $\boldsymbol{v}_{\mathrm{cl}}$ is the corresponding climatological velocity, and $\rho_0 = 1{,}027$ kg/m^3 is the mean sea water density. It should be noted that the definition of the eddies (7) in terms of the zero time-mean component of the flow may contain significant signal associated with transient flow features on the larger scales (i.e., not necessarily eddy-like structures). Although a more consistent scale separation can be derived by employing additional averaging in space (e.g., Wang et al. 2001), we will still follow the time-averaged version (7), keeping in mind that EKE also contains KE of the transient larger scale features.

The 18-year mean EKE distribution in the upper 300 m of the Bering Sea is shown in Fig. 8. As expected, enhanced eddy activity is observed in the KC and AS regions. Obviously, it is partly associated with the above-mentioned transient features of these large-scale currents. Less intensive but persistent eddies are also present north of the Aleutian Arc in the regions of the main inflow passages and along the continental slope controlling the BSC pathway (Mizobata et al. 2002, 2006).

Time evolution of the mean EKE at 20, 187 and 900 m is shown in Fig. 9. The seasonal cycle is more pronounced

at the intermediate depth (150 m) with the maxima observed in March-April, exhibiting a 2-month delay with respect to the maximum large-scale currents observed in January (cf. Fig. 5). On the longer term, there is a signature of a trend whose magnitude ranges between 0.5 % (at 50 m) and 1 % (900 m) of the mean EKE per year. Although long-term trends in the upper layers are not statistically confident because of the strong variability on seasonal and shorter time scales, the EKE trend below 700 m is apparent (lower curve in Fig. 9).

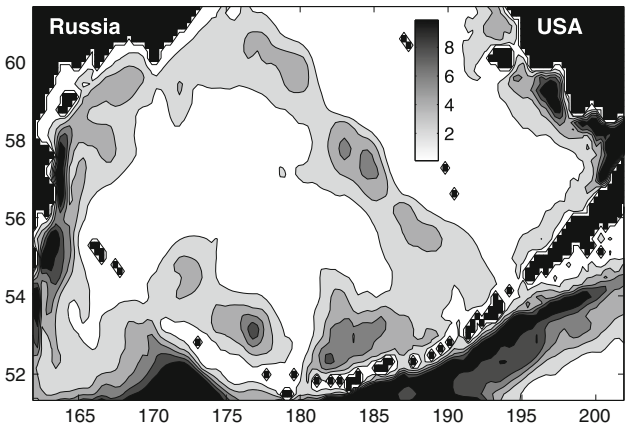

Fig. 8 Horizontal distribution of the eddy kinetic energy (J/m^3) averaged in the 0–300 m water column

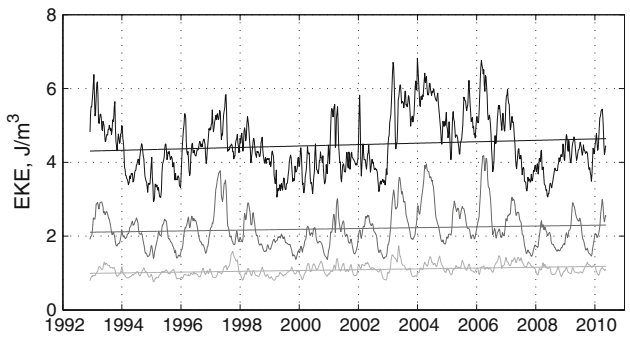

Fig. 9 Evolution of the BS eddy kinetic energy at (from *top* to *bottom*) 20, 187 and 900 m averaged for the domain show in Fig.1. *Thin straight lines* show the long-term trends

Long-term variations of the EKE in the Bering Sea also exhibit significant correlations with the PDO index (Mantua et al. 1997). Figure 10 demonstrates the evolution of the Bering Sea EKE averaged in the upper 1,000 m and the PDO index. The quantities have correlation 0.49 at the 95 % confidence level under the assumption of statistical independence of the bimonthly values. Even larger (0.54) correlation is observed between PDO and EKE averaged over the BSC region (quadrangle 3 in Fig. 2a). It is noteworthy that correlations between the rms gradients of the Aviso SSH anomalies and PDO index are much smaller, indicating the validity of the presented reconstruction of the velocity field in the deeper layers.

Positive correlations between the eddy activity in the BS basin and the PDO index indicate an atmospheric teleconnection between the North Pacific SST anomalies and the BS circulation. During the positive PDO anomalies there is an increase of the large-scale poleward temperature gradient in the lower troposphere, which intensifies cyclonic circulation in the Aleutian low of the North Pacific (e.g., Wang et al. 2004). The latter amplifies oceanic cyclonic gyres, including the BS large-scale circulation pattern (Fig. 1), which in turn causes enhanced eddy activity. In particular, Schumacher and Reed (1992), Cokelet and Stabeno (1997) observed that BS mesoscale currents may reach up to 80 cm/s in magnitude and penetrate to the depth of at least 500 m along the eastern Alaskan continental slope. Such a strong eddy activity results in the enhanced transport of nutrients from the deep regions onto the eastern BS shelf (Stabeno et al. 1999) and explains higher biological production (Hare et al. 1999) in the BS during the positive PDO anomalies.

The diagnosed correlation between PDO and the BS eddies supports this hypothesis and provides another indication of the coherence between the BS circulation and the NP currents on the interannual time scales.

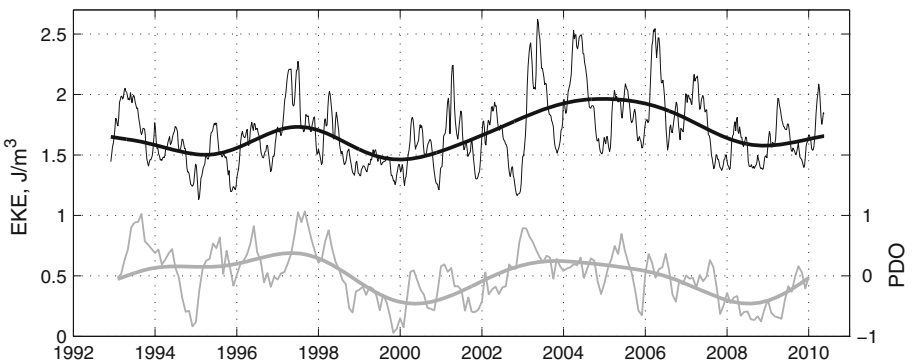

Fig. 10 Depth-averaged eddy kinetic energy in the upper 1,000 m (*black lines*, *left axis*) and the PDO index (*gray lines*, *right axis*). The low-pass filtered series are shown in *bold* and have a cross correlation of 0.49

4 Discussion and conclusions

The presented quantitative estimate of the 3d BS circulation in 1992–2010 is the first attempt at such a reconstruction that heavily relies on the massive satellite observations of the sea surface height. To reduce the uncertainty in the mean SSH, we used the mean dynamic topography obtained from the 4dVar assimilation of the hydrographic, drifter and atmospheric data into the regional numerical model (Panteleev et al, 2006, 2011). Such an approach allowed us to reduce the absolute SSH errors to a few centimeters (Fig. 2b) and accurately estimate the mean seasonal cycle of the BS density field. To assess the mesoscale density anomalies, we employed the Cooper-Haines scheme, and then diagnosed the velocity field using the geostrophic and hydrostatic relationships.

The technique may poorly resolve only the density field component driven by interannual variations in atmospheric forcing, which may cause significant changes in the large-scale water mass structure and potential vorticity. We believe, however, that these effects are not dominant within the 18-year period under consideration and have only a marginal impact on the quality of the reconstructed circulation. This assumption has been validated by the direct comparison with subsurface and deep velocity observations by drifters, which demonstrated a reasonable agreement between the reconstructed velocities and the data (see Table 1; Figs. 4, 5).

Analysis of the BS circulation in 1992–2010 provided the following mean transports for the major currents: the Alaskan Stream 24.3 ± 6.7 Sv, the Kamchatka Current 22.1 ± 6.3 Sv, the Near Strait 11 ± 3.9 Sv and the Bering Slope Current 7.3 ± 2.8 Sv. The AS and KC were diagnosed to have undercurrents below 2 km with the transports of −4.1 ± 1.2 and −2.9 ± 0.8 Sv, respectively, so that their transports in the upper 2 km exceed 28 and 24 Sv. Overall, the obtained estimates indicate that the BS current system has a considerably higher magnitude than previously thought. This is partly due to the fact that most of the estimates known in the literature were obtained from diagnostic calculations relative to 1,000–1,500 db. New data from Argo drifters (Table 1; Fig. 4) indicate that deep currents do significantly contribute to the total transport of the BS currents.

At the seasonal scale, significant amplification of the BS current system is observed in winter, with the maximum in December–January (Fig. 6), which is followed by the EKE maximum in March-April. The mean seasonal magnitudes of the BS currents are diagnosed as 6 Sv for the AS, 8 Sv for the KC, 4 Sv for the NS and 3 Sv for the BSC.

All the currents exhibited significant positive correlations with the AS transport on intra-annual time scale. Lagged correlation analysis revealed increasing time lags of the maximum transport correlations between the AS and currents (BSC and KC) located further downstream the BS cyclonic gyre. A significant negative correlation between AS and NS transports has also been found. These results support the concept that the BS basin is ventilated by the waters, carried by the AS south of the Aleutian Arc and by the flow through the Near Strait. In particular, the Near Strait inflow amplifies when the upstream AS is relatively weak, resulting in stronger recirculation in the western BS. Stronger AS appears to reduce the Near Strait inflow and at the same time produces larger transport through the Aleutian Arc, which amplifies the main cyclonic gyre controlled by the continental slope within the BSC region.

The correlation analysis allowed proposing simple statistical relationships between the inflow NS and AS transports and transports of the currents contributing to the BS cyclonic gyre (KC and BSC). The relationships explain 89 and 77 % of the KC and BSC transport varaibility and could be useful for hindcasting/forecasting the circulation of the BS gyre.

Correlations with the direct observations of the Bering Strait throughflow were found to be statistically insignificant on the interannual scale, whereas on the intra-annual scales significant (−0.44 to −0.35) negative correlations were observed for all the currents with an exception of the BSC. The result is due to the fact that the Bering Strait outflow reaches its maximum in late summer (Roach et al. 1995), whereas the BS circulation has a tendency to spin up in winter. A possible reason for this is that the Bering Strait outflow is generally controlled by the wind forcing and shallow water dynamics on the vast shelf of the northern BS, which was not considered in the present study because of the lack of altimeter data over the ice.

Analysis of the eddy kinetic energy revealed a statistically confident long-term trend of approximately 0.01 J/m^3/year for the depth-integrated EKE, which is most prominently seen at depths below 800 m (Fig. 9). Although our definition of EKE also includes transient larger-scale currents, the revealed trend clearly indicates the increasing volatility of the Bering Sea circulation, characteristic for climate transitions. Both EKE and major current transports in the BS exhibit fairly strong correlation with the PDO index, thus showing that the Bering Sea basin is tightly connected to the NP dynamics on a larger scale.

The major drawback of the present study is the absence of integral mass balance, which can further constrain the density field diagnosed from the well-observed surface pressure. Introducing horizontal viscosity in the diagnostic equations and modifying the Cooper-Haines algorithm by prescription of zero normal velocity at the bottom may bring more realism to the reconstruction.

Acknowledgments This study was supported by the Japan Agency for Marine-Earth Science and Technology (JAMSTEC) through their sponsorship of research activities at the International Arctic Research Center and by the Office of Naval Research (Program element 0602435N, project "Observational Impact"). G. Panteleev was also supported by the National Science Foundation 1107925 award and by the North Pacific Research Board (NPRB) 828 award. D. Nechaev was supported by the NPRB 828 award.

References

Clement Kinney J, Maslowski W, Okkonnen SR (2009) On the processes controlling shelf-basin exchange and outer shelf dynamics in the Bering Sea. Deep Sea Res II 56(17):1351–1376

Cherniawsky JY, Foreman MGG, Crawford WR, Beckley BD (2004) Altimeter observations of sea level variability off the West Coast of North America. Int J Remote Sensing 25:1303–1306

Cherniawsky JY, Crawford WR, Nikitin O, Carmack E (2005) Bering Strait transports from satellite altimetry. J Mar Res 63:887–900

Clement JL, Maslowski W, Cooper LW, Grebmeier JM, Walczowski W (2005) Ocean circulation and exchanges through the northern Bering Sea19792001: model results. Deep Sea Res II 52(17): 3509–3540

Cokelet ED, Schall ML, Dougherty DM (1996) ADCP-refrenced geostrophic circulation in the Bering Sea basin. J Phys Oceanogr 26(7):1113–1128

Cokelet ED, Stabeno PJ (1997) Mooring observations of the thermal structure, density stratification and currents in the southeast Bering basin. J Geophys Res 102(C10):1113–1128

Cooper M, Haines K (1996) Altimetric assimilation with water property conservation. J Geophys Res 101:1059–1077

Elmann A (2010) Validation of the new Earth Gravitational Model EGM08 over the Baltic countries. Gravity, Geoid and Earth Observation International Association of Geodesy Symposia, vol 135, part 6, pp 489–496. doi:10.1007/978-3-642-10634-7

Fomin LM (1964) The dynamic method in oceanography. Elsevier Oceanogr Series, vol 2, p 212

Foreman M, Bell RG, Cherniawsky JY, Beckley B (2004) Tides and sea-level variability in the south-west Pacific from TOPEX/ Poseidon. N Z J Mar Freshw Res 38:649–669

Johnson GC, Stabeno PJ, Riser SC (2004) The Bering Slope Current revisited. J Phys Oceanogr 34(2):384–398

Hare SR, Mantua NJ, Francis RC (1999) Inverse production regimes: Alaskan and West Coast Salmon. Fisheries 24(1):6–14

Hogg A, Killworth PD, Blundell JR (2005) Mechanisms of decadal variability of the wind-driven ocean circulation. J Phys Oceanogr 35:512–531

Hu H, Wang J (2010) Modeling effects of tidal and wave mixing on circulation and thermohaline structures in the Bering Sea: process studies. J Geophys Res 115:C01006. doi:10.1029/2008 JC005175

Hughes FW, Coachman LK, Aagard K (1974) Circulation transport and water exchange in the western Bering Sea. In: Hood DW, Kelly EJ (eds) Oceanography of the Bering Sea with emphasis of the renewable resources. Inst. of Mar. Sci., Univ. of Alaska Fairbanks, Fairbansk, pp 59–98

Ladd C, Stabeno P (2009) Freshwater transport from the Pacific to the Bering Sea through the Amukta Pass. Geophys Res Lett 36:L14608.doi:10.1029/2009GLO039095

Luchin VA, Semiletov IP, Weller GE (2002) Changes in the Bering Sea region: atmosphere–ice–water system in the second half of the twentieth century. Prog Oceanogr 55(1–2):23–44

Mantua NJ, Hare SR, Zhang Y, Wallace JM, Francis RC (1997) A Pacific interdecadal climate oscillation with impacts on salmon production. Bul Am Meteorol Soc 78:1069–1079

Maslowski W, Roman R, Kinney JC (2008) Effects of mesoscale eddies on the flow of the Alaskan Stream. J Geophys Res 113:C07036. doi:10.1029/2007JC004341

Mizobata K, Saitoh SI, Shiomoto A, Miyamura T, Shiga N, Imai K, Toratani M, Kajiwara Y, Sasaoka K (2002) Bering Sea cyclonic and anticyclonic eddies observed during summer 2000 and 2001. Prog Oceanogr 55:65–75

Mizobata K, Wang J, Saitoh SI (2006) Eddy-induced cross-slope exchange maintaining summer high productivity of the Bering Sea shelf break. J Geophys Res 111:C10017. doi:10.1029/2005 LC003335

Mizobata K, Shimada K, Woodgate R, Saitoh S-I, Wang J (2010) Estimation of heat flux through the eastern Bering Strait. Geophys Res Lett 37:405–424

Okkonen SR (1996) The influence of an Alaskan Stream eddy on flow through Amchitka Pass. J Geophys Res 101:8839–8851

Overland JE, Stabeno P (2004) Is the climate of the Bering Sea warming and affecting the ecosystem? EOS 85(33):309–312

Panteleev G, Stabeno P, Luchin VA, Nechaev D, Ikeda M (2006) Summer transport estimates of the Kamchatka Current derived as a variational inverse of hydrophysical and surface drifter data. Geophys Res Lett 33:L09609. doi:10.1029/2005GL024974

Panteleev G, Yaremchuk M, Stabeno P, Luchin V, Nechaev DA, Kukuchi T (2011) Dynamic topography of the Bering Sea. J Geophys Res 116:C05017. doi:10.1029/2010JC006354

Pascual A, Faugre Y, Larnicol G, Le Traon P-Y (2006) Improved description of the ocean mesoscale variability by combining four satellite altimeters. Geophys Res Lett 33:L02611. doi:10.1029/ 2005GL024633

Reed RK (1984) Flow of the Alaskan Stream and its variations. Deep Sea Res 31(4):369–386

Reed RK, Khen GV, Stabeno PJ, Verkhunov AV (1993) Water properties and flow over the deep Bering Sea basin, summer 1991. Deep Sea Res 40:2325–2334

Roach AT, Aagaard K, Pease CH, Salo SA, Weingartner T, Pavlov V, Kulakov M (1995) Direct measurements of transport and water properties through Bering Strait. J Geophys Res 100:18443–18457

Schreier PJ (2008) A unifying discussion of correlation analysis for complex random vectors. IEEE Trans Signal Proc 56(4):1327–1336

Schumacher JD, Reed RK (1992) Characteristic of current over the continental slope of the eastern Bering Sea. J Geophys Res 97:607–623

Stabeno, Reed (1992) Stabeno PJ, Reed RK (1992) A major circulation anomaly in the Western Bering Sea. Geophys Res Lett 19:1671–1674

Stabeno PJ, Reed RK (1994) Circulation in the Bering Sea basin observed by satellite-tracked drifters: 1986–1993. J Phys Oceanogr 24:848–854

Stabeno PJ, Schumacher JD, Ohtani K (1999) The physical oceanography of the Bering Sea. In: Dynamics of the Bering Sea. Alaska Sea Grant College Program, Fairbanks

Stabeno PJ, Kachel DG, Sullivan ME (2005) Observation from moorings in the Aleutian Passes: temperature, salinity and transport. Fish Oceanogr 14(Suppl. 1):39–54

Verkhunov AV, Tkachenko YY (1992) Recent observations of variability in the Western Bering Sea current system. J Geophys Res 97(C9):14369–14376

Wang J, Ikeda M (1997) Diagnosing ocean unstable baroclinic waves and meanders using the quasigeostrophic equations and the Q-vector method. J Phys Oceanogr 27:1158–1172

Wang J, Jin M, Patrick EV, Allen JR, Eslinger DL, Mooers CNK, Cooney RT (2001) Numerical simulations of the seasonal circulation patterns and thermochaline structures in the Prince William Sound, Alaska. Fish Oceanogr 10(suppl. 1):132–148

Wang J, Jin M, Musgrave DL, Ikeda M (2004) A hydrological digital elevation model for freshwater discharge into the Gulf of Alaska. J Geophys Res 109:C07009. doi:10.1029/2002JC001430

Wilson S (2000) Launching the ARGO armada. Oceanus 42(1):17–19

Woodgate RA, Aagaard K, Weingartner T (2005) Monthly temperature, salinity, and transport variability of the Bering Strait through flow. Geophys Res Lett 32:L04601. doi:10.1029/2004GL021880

Zhang Y, Pedlosky J, Flierl GR (2011) Cross-shelf and out-of-bay transport driven by an open-ocean current. J Phys Oceanogr 41:2168–2185